Experimental stabilisation of 2D vortex patterns using time-dependent forcing

A Letters Journal Exploring the Frontiers of Physics

October 2013

EPL, **104** (2013) 24003
doi: 10.1209/0295-5075/104/24003

www.epljournal.org

Experimental stabilisation of 2D vortex patterns using time-dependent forcing

M. Lauret[1,2(a)], L. P. J. Kamp[3], G. J. F. van Heijst[3], M. R. de Baar[1,2] and H. Nijmeijer[4]

[1] *FOM Institute DIFFER - Dutch Institute for Fundamental Energy Research, Association EURATOM-FOM, Trilateral Euregio Cluster - P.O. Box 1207 Nieuwegein, The Netherlands*
[2] *Control Systems Technology, Department of Mechanical Engineering - Eindhoven University of Technology P.O. Box 513, 5600 MB Eindhoven, The Netherlands*
[3] *Fluid Dynamics Laboratory, Department of Applied Physics - Eindhoven University of Technology Eindhoven, The Netherlands*
[4] *Dynamics and Control, Department of Mechanical Engineering - Eindhoven University of Technology Eindhoven, The Netherlands*

received 9 September 2013; accepted in final form 28 October 2013
published online 19 November 2013

PACS 47.32.C- – Vortex dynamics
PACS 47.20.-k – Flow instabilities
PACS 47.27.De – Coherent structures

Abstract – Experimental results of the effect of time-periodic and "chirped" (electro-magnetic) forcing on vortex patterns in shallow-water-layer flows are presented. Analogously to vibrational control, the use of a time-periodic forcing results in stabilisation of otherwise unstable vortex patterns. Chirped frequency forcing yields self-organising patterns that are different from those in stationary and periodically forced experiments. The results are shown to be consistent with theoretical analysis of 2D Taylor-Green vortices, *i.e.* unstable analytical solutions of the 2D Navier-Stokes equation. These results imply that, compared to the more often analysed stationary forced flows, time-varying forcing can stabilise different vortex patterns in shallow-water-layer flows.

Introduction. – Shallow fluid flows behave quite differently from fully three-dimensional (3D) flows. Contrary to the small length scales observed in 3D turbulence, these quasi–two-dimensional (Q2D) flows typically self-organise into large vortices [1–4]. Self-organisation is, for example, seen in geophysical flows (both in the atmosphere and in the oceans), in soap films, and in electromagnetically forced shallow-water-layer experimental setups. If 3D effects are completely negligible, these flows can be modelled by the two-dimensional (2D) Navier-Stokes equation.

The Q2D behaviour of cellular flows (square arrays of vortices in a bounded domain) has been studied extensively. These flows are experimentally realised in conductive shallow fluid layers using electromagnetic forcing [5–7]. Contrary to the self-organisation in decaying Q2D flows, stationary forced flows attain a stationary state that is organised for moderate forcing amplitudes [8]. However, if the forcing amplitude is increased, the flow typically undergoes a bifurcation, consistent with theoretical analysis [9], and becomes time-periodic and eventually chaotic in time and spatially disorganised.

For certain cases, Q2D cellular flows can be described analytically as 2D Taylor-Green vortices [10]. These square vortex arrays are a family of exact solutions of the 2D Navier-Stokes equation. Their stability depends on several factors like boundary conditions, the value of the Reynolds number and magnitude and type of the forcing. Stability analysis for decaying and stationary forced 2D Taylor-Green vortices have revealed that the vortices remain stable for small Reynolds numbers [11–14]. For decaying Taylor-Green vortex arrays at a higher Reynolds number, the self-organisation into a domain filling vortex can be explained using variational techniques [15,16].

In the present paper, we report on an experimental study of the influence of different types of forcing on the stability and self-organisation of Q2D cellular flows. In particular the effect of time-varying forcing is discussed. We show that time-periodic forcing can stabilise a cellular flow that is similar to a 2D Taylor-Green vortex pattern, but different from the Taylor-Green vortex resulting from

(a) E-mail: m.lauret@tue.nl

a stationary forcing with the same spatial length scale as the time-periodic one.

The remainder of this paper is organised as follows. After describing the experimental setup, experiments in which the flow is forced constantly in time are presented. Then, experimental results for time-periodic forcing are discussed. To study the effect of aperiodic-in-time forcing, the flow resulting from "chirp" forcing (*i.e.* with the temporal frequency of the forcing changing during the experiment) is studied. Next, the experimental results are modelled with analytical solutions of the 2D vorticity equation. In the discussion, the comparison between the theoretical analysis and the experiments, and also the role of the forcing in vortex stabilisation are discussed. Finally, some conclusions will be drawn.

Experimental setup. – The experimental setup (described in more detail in [8]) consists of a square tank with length $L_0 = 0.52\,\mathrm{m}$, filled with a NaCl-water solution with depth $H = 8.5\,\mathrm{mm}$. The water has a density $\rho = 1142\,\mathrm{kg/m^3}$ and a kinematic viscosity $\nu = 1 \cdot 10^{-6}\,\mathrm{m^2/s}$. The surface flow is described in a Cartesian right-handed coordinate system (x, y) and the z-axis is perpendicular to the fluid surface.

Beneath the bottom, 100 permanent magnets of 1.1 T are arranged in a square 10×10 configuration with alternating polarity, resulting in a magnetic field $\mathbf{B}(x, y, z)$. The distance between two neighbouring magnets is $l = 5\,\mathrm{cm}$.

On opposite sides of the tank, two electrodes create a voltage difference that drives an electric current $I(t)$, whose magnitude can be varied between $\pm 1\,\mathrm{mA}$ and $\pm 7\,\mathrm{A}$. The flow is forced by a Lorentz force $\mathbf{F}_L$, resulting from the combination of the magnetic field $\boldsymbol{B}(x, y, z)$ and the uniform electric current density $\mathbf{J}(t) = J(t)\mathbf{e}_x$, where $\mathbf{e}_x$ is the unit vector in the x-direction. The magnetic field is assumed to be predominantly perpendicular to the fluid surface and z-independent, implying $\mathbf{B}(x, y) = B(x, y)\mathbf{e}_z$ (where $\mathbf{e}_z$ is the unit vector in the z-direction). The Lorentz force is then given by

$$\mathbf{F}_L(x, y, t) = \frac{1}{\rho}\mathbf{J} \times \mathbf{B} = -\frac{1}{\rho}J(t)B(x, y)\mathbf{e}_y, \qquad (1)$$

where $\mathbf{e}_y$ is the unit vector in the y-direction. It should be noticed that this Lorentz force is strongly localised around the magnets.

To visualize the flow, small tracer particles (diameter $250\,\mu\mathrm{m}$) float on the free fluid surface. These moving particles are recorded by a camera mounted above the setup. This camera has a sample rate of 15 frames/s and the camera records the flow in a $L \times L$ square area in the middle of the tank, with $L = 17.5\,\mathrm{cm}$. The flow can then be visualised with streak-line figures. By applying particle image velocimetry (PIV) [17], the 2D velocity fields $\mathbf{v}(x, y, t) = [u, v]^T$ can be determined. From these velocity fields the vorticity $\omega = (\nabla \times \mathbf{v}) \cdot \mathbf{e}_z = \partial v/\partial x - \partial u/\partial y$, the kinetic energy $E(t) = \frac{1}{2}\int_{\mathcal{D}} |\mathbf{v}|^2 \mathrm{d}A$, and the enstrophy $\Omega(t) = \frac{1}{2}\int_{\mathcal{D}} \omega^2 \mathrm{d}A$ can be determined, with $\mathcal{D}$ denoting the $L \times L$ area at the fluid surface.

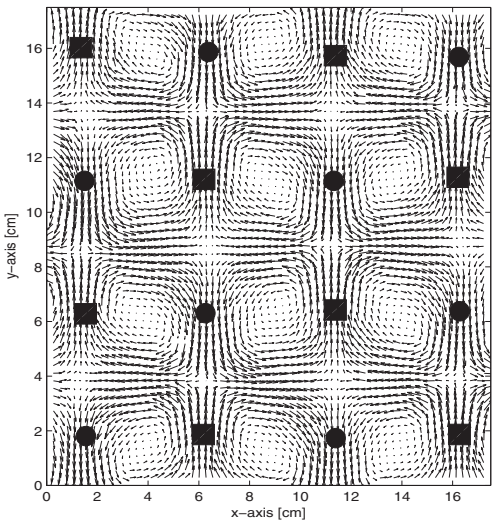

Fig. 1: Experimentally obtained flow field (vectors denote the instantaneous velocity) with 100 magnets and a direct current $I = 20\,\mathrm{mA}$. The array of alternating, permanent magnets is indicated by the black circles (magnetic field pointing upwards) and squares (magnetic field pointing downwards). For a direct current this gives rise to an alternating Lorentz force resulting in a square array of vortices each having alternating vorticity.

Experimental observations. – To study the influence of the forcing on the phenomenology of emerging vortex patterns, experiments with different types of Lorentz forcing have been carried out. The first experiment studies the effect of a direct current (DC) of 20 mA. This forcing results in a square array of vortices each having a size of $l = 5\,\mathrm{cm}$, as shown in fig. 1. This is similar to observations by Cieślik *et al.* [8]. The vortex pattern, with approximately 3×4 vortices in the viewing area, remains stable for currents up to $I = 40\,\mathrm{mA}$.

A distinctly different vortex pattern is observed when the flow is forced with a time-periodic Lorentz force. Applying an alternating current (AC) given by $I(t) = I_0 \sin(2\pi f t)$ (with amplitude I_0[A] and frequency f[Hz]) results in the vortex pattern shown in fig. 2. In this figure, snapshots of the velocity field for $f = 1\,\mathrm{Hz}$ and $I_0 = 5\,\mathrm{A}$ are shown at three different time instances. Vortex arrays emerge that have not been observed using a stationary forcing. It has been experimentally verified that for $0.5 < f < 5\,\mathrm{Hz}$ and $1 < I_0 < 7\,\mathrm{A}$, the observed vortex array is always similar to the ones shown in fig. 2. From fig. 2 we conclude that most of the time the flow field is represented by a spatially periodic pattern of vortices, each having a size that is half the size of the vortices produced with a direct current, *i.e.* 2.5 cm, as depicted in fig. 2(b) and fig. 3. Moreover, this vortex array remains intact for amplitudes of the alternating current up to $I_0 = 7\,\mathrm{A}$, which is far above the maximum direct current (together with a suitable array of magnets) that can be used to produce such a vortex pattern that is stable.

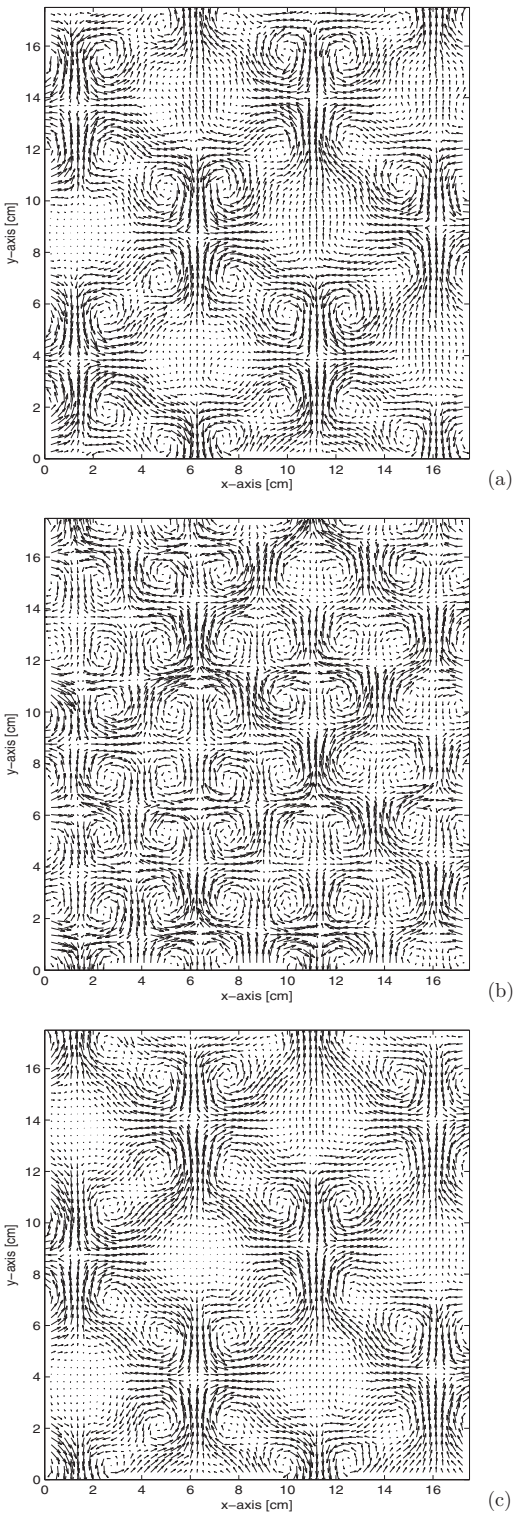

Fig. 2: Velocity fields of an experiment with an alternating current according to $I = 5\sin(2\pi t)$ A. During one period (1 s) the velocity field evolves between the shown vortex patterns, *i.e.* according to the sequence a-b-c-b-a.

To also investigate vortex pattern formation for more general forcing protocols, an aperiodic electric current has been applied. More specifically, experiments have been carried out in which the current is given by $I_{chirp}(t) = I_0(t)\sin(2\pi\cdot 10^{-5}t^3)$, where $I_0(t) = 9\cdot 10^{-5}t^2$ and an additional saturation bound $|I_0(t)| \leq 7$ A holds. This so-called "chirp" current has a slowly varying amplitude and frequency. The current specified above is used for a 500 s long experiment and after 279 s the amplitude sometimes saturates at ± 7 A. The resulting maximum chirp frequency is approximately 7.5 Hz. Two experiments witch such chirp forcings have been carried out: one with a chirp current with increasing frequency, and another one where the instantaneous frequency decreases in time (inverse chirp current given by $I_{chirp}(t-500)$). Both experiments show comparable phenomena.

Fig. 3: Snapshot of the streak-line pattern corresponding to fig. 2(b).

In both the chirp experiments and the inverse chirp experiment, a vortex pattern appeared, as shown in fig. 4, with a different symmetry from that in the former experiments. It is observed that the large $l = 5$ cm vortices are now aligning diagonally and, contrary to the pattern in fig. 1, only half of the domain is filled by these counter-clockwise rotating large vortices. Between the large vortices, small and weak clock-wise rotating vortices emerge. This new vortex pattern remains clearly visible for more than 10 s, during which time the large vortices keep rotating in the same direction.

The flow regime of the experiments can be characterised by two dimensionless parameters. The Reynolds number $Re = Ul/\nu$, characterising the ratio between advective and viscose forces, is typically of order $Re = 100$ for all experiments, as the mean velocity U is typically $U \approx 2\cdot 10^{-3}$ m/s. This means that the nonlinear effect of advection cannot be neglected, but also that the flow is not turbulent. The relative importance of the forcing can be characterised by the Chandrasekhar number [18] $Ch = IBH/\rho\nu^2$, which varies for the different experiments. The experiment with $I = 20$ mA has $Ch = 1.5\cdot 10^5$. But in both the periodic experiment, with $|I| = 5$ A, and the chirping experiment, with $\max(I) = 7$ A the forcing is significantly more dominant, as the Chandrasekhar number is higher, respectively $Ch = 3.0\cdot 10^7$ and $Ch = 5.2\cdot 10^7$.

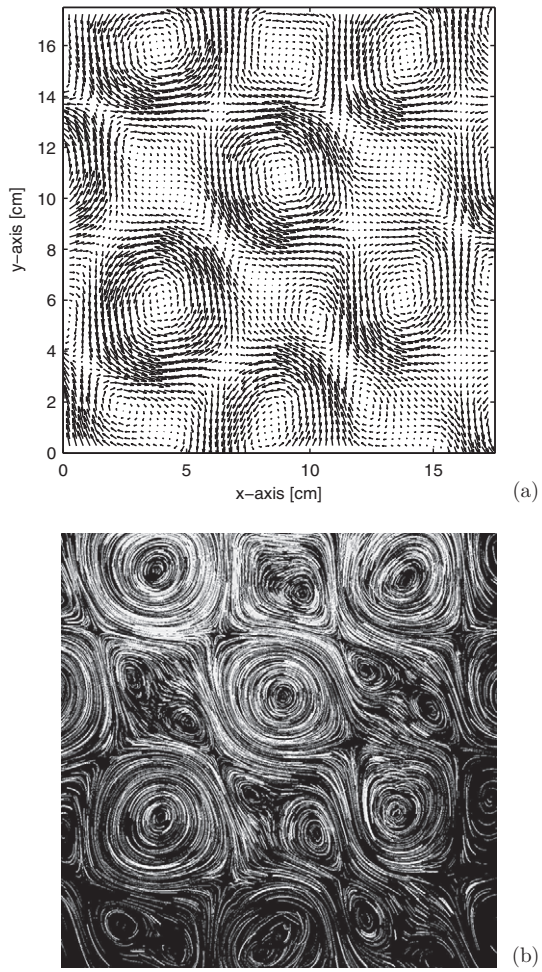

Fig. 4: Velocity field (a) and streak-lines (b) of an experiment with an inverse chirp forcing. The vortex pattern contains both large (counterclockwise rotating) and small vortices.

Discussion. – Flows in shallow fluid layers are often assumed to be quasi–two-dimensional and therefore governed by the 2D Navier Stokes equations. Recent work, however, has shown that 3D effects can play a significant role in this type of flows [19]. Nevertheless, in the present study we assume vertical velocities inside the fluid layer as well as free surface deformations to be negligible and therefore consider the observed surface flow to be governed by the 2D Navier-Stokes equation for an incompressible fluid. Alternatively, we consider the vorticity-stream function formulation of the Navier-Stokes equation, which is given by

$$\frac{\partial \omega}{\partial t} + (\mathbf{v}\cdot\nabla)\omega = \nu\nabla^2\omega - \kappa\omega + F_\omega, \tag{2a}$$

$$-\nabla^2\psi = \omega, \tag{2b}$$

where ν is the kinematic viscosity and F_ω denotes the z–component of the curl of the body force acting upon the fluid. ψ is the stream function that is defined through $\mathbf{v} = \nabla\psi \times \nabla z$. Viscous dissipation due to bottom friction, which is the dominant dissipation mechanism for shallow flows above a no-slip bottom, can be modelled assuming a Poiseuille-like vertical profile for the horizontal flow field, resulting in the Rayleigh bottom friction term $\kappa\omega$, where $\kappa = \nu\pi^2/4H^2 = 0.038\,\mathrm{s}^{-1}$.

The recorded surface flows, depicted in figs. 1, 2 and 3, are now modelled as 2D Taylor-Green vortices [10,20], which are solutions of the eigenvalue problem $-\nabla^2\psi_{m,n} = \omega_{m,n} = \lambda_{m,n}\psi_{m,n}$ and $\psi_{m,n}$ (and consequently $\omega_{m,n}$ too) is assumed to vanish at the boundary of $L\times L$ domain. Due to the linear relationship between ω and ψ, the nonlinear advection term in eq. (2a) cancels, thus rendering this equation linear and exactly solvable for an unforced flow with initial condition $\omega(x, y, t = 0) = c\omega_{m,n}(x, y)$ by

$$\omega(x, y, t) = c\omega_{m,n}(x, y)e^{-(\nu\lambda_{m,n}+\kappa)t}, \tag{3}$$

where $\omega_{m,n}$ is given by

$$\omega_{m,n} = \sin(m\pi x/L)\sin(n\pi y/L) \tag{4}$$

and c is a constant. For sufficiently small initial amplitudes c of these Taylor-Green vortices (*i.e.* for a small Reynolds number) this exponentially decaying solution (4) is stable for finite disturbances [12]. For larger initial amplitudes, the vorticity tends to evolve towards a big domain filling vortex, described by the first Taylor-Green vortex $\omega_{1,1}$ [15,16].

In order to compare the experimentally observed vortex patterns with the Taylor-Green vortices, we consider the ratio between enstrophy and energy Ω/E, which plays an important role in the subsequent analysis. This ratio is minimised by the smallest eigenvalue of the eigenvalue problem mentioned before, *i.e.* $\lambda_{1,1} \leq \Omega/E$, and this minimum is achieved when $\omega = \omega_{1,1}$ [15,16]. Moreover, by using Green's first identity one can prove that $\Omega/E = \lambda_{m,n}$ for every Taylor-Green vortex $\omega_{m,n}$ [15]. According to (4) this implies that patterns with smaller vortices dissipate faster.

In order to evaluate the adequacy of the Taylor-Green vortex patterns for describing the experimentally observed vortex patterns, we consider the 2D parameter space spanned by energy and enstrophy. In this parameter space a Taylor-Green vortex pattern given by $\omega_{m,n}$ is represented by a straight line with slope $\lambda_{m,n}$ through the origin (see fig. 5). The vortex pattern shown in fig. 1 and resulting from stationary (DC) forcing strongly resembles the Taylor-Green vortex pattern described by $\omega_{3,4}$, which also is a stationary solution to eq. (2b) provided $F_\omega = F^{3,4} := c\sin(3\pi x/L)\sin(4\pi y/L)$ with an appropriate value of the constant c. This solution is stable for small forcing amplitude c and small Reynolds number [11], whereas bottom friction tends to increase the stability range [14]. The temporal evolution of the experimentally obtained ratio Ω/E has also been plotted in fig. 5 at discrete time instances. Obviously, for this experiment Ω/E is approximately constant in time and close to the theoretical value, which is given by $\lambda_{3,4} \approx 0.81$. Therefore, it can be concluded that the applied stationary

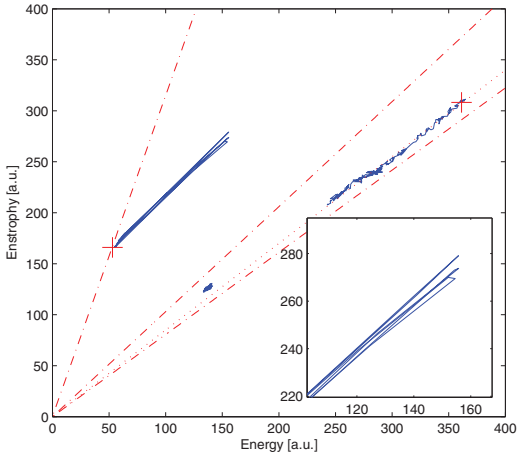

Fig. 5: (Colour on-line) The experimental E, Ω evolution. The slope of the three dash-dotted lines equals the eigenvalues $\lambda_{3,4} = 0.81$, $\lambda_{4,4} = 1.03$ and $\lambda_{7,7} = 3.15$, in increasing order. The dashed line has a slope of 0.85 and the inverse chirp experiment (which starts at the plus symbol) evolves on this diagonal. The point cloud, around $E = 140$, $\Omega = 120$, corresponds to the stationary 20 mA experiment. The solid line at $E = 150$, $\Omega = 250$ corresponds to several periods of the periodically forced experiment. The zoom box indicates that, for a time-periodic forcing, E and Ω are not monotonously decreasing but oscillating between $(E, \Omega) \approx (160, 280)$ and $(E, \Omega) \approx (55, 165)$. All experimental data is plotted as blue.

forcing stabilises the stationary Taylor-Green vortex $\omega_{3,4}$. Note, however, that the forcing used in the experiments, as defined in eq. (1), is strongly localised around the magnets and is really different from the type of forcing that is commonly used or assumed in studies [13,21] and also different from the theoretical forcing $F^{3,4}$ mentioned before. Consequently, the formation of the vortex pattern is a more complex process [5,8,21] in which the advection term does play an essential role and for which no analytical solution is known. However, in a steady state the vorticity advection term appears to be negligible, in view of the strong resemblance between the Taylor-Green solution $\omega_{3,4}$ and the experimentally observed vortex pattern.

The experiments with a periodic (AC) forcing resulted in vortex patterns that most of the time are akin to another Taylor-Green vortex $\omega_{7,7}$, see fig. 2 and fig. 3. Reasoning as in the previous paragraph suggests the periodic forcing $F_\omega = F^{7,7} := c \sin(2\pi f t) \sin(7\pi x/L) \sin(7\pi y/L)$, with $f = 1$ as a candidate forcing protocol for creating this pattern. However, there is one caveat: the periodic forcing $F^{7,7}$ leads to a solution of eq. (2a) that has the form $c_2 \sin(2\pi f t - \phi)\omega_{7,7}$, with constants c_2 and ϕ. In this solution individual vortices periodically change their rotation direction, as opposed to the experimentally observed vortices in fig. 2 and fig. 3. Therefore, the observed vortex pattern is essentially different from the one created by $F^{7,7}$ and there appears to be no obvious analytical solution similar to the observed vortex pattern. This is due to the strong localisation of the Lorentz force around the magnets, as this forcing does not resemble a pure Taylor-Green mode. Nevertheless, the relevance of $\omega_{7,7}$ for mimicking the experimentally observed vortex pattern for the AC forcing case becomes even more convincing when considering the temporal evolution of the experimentally obtained enstrophy and energy. As time progresses, the ratio of these two quantities commutes between two points in the parameter space shown in fig. 5 and in more detail in the zoom box. The states represented by figs. 2(a) and (c) both correspond to a point in the parameter space that is approximately given by $(E, \Omega) = (160, 280)$ whereas the vortex pattern shown in fig. 2(b) corresponds approximately to $(E, \Omega) = (55, 165)$, which is close to the theoretical eigenvalue $\lambda_{7,7} \approx 3.15$ associated with the Taylor-Green vortex pattern $\omega_{7,7}$. Since the time-averaged vortex pattern as defined by $\bar{\omega} = 1/T \int_0^T \omega dt$, where ω is the experimentally obtained vorticity, is approximately equal to $\omega_{7,7}$, see also fig. 2, we conclude that periodic (AC) forcing of the flow stabilises a Taylor-Green vortex pattern represented by $\omega_{7,7}$. This is a remarkable result in view of the fact that experimental realisation of such a pattern using stationary forcing (and adequate spacing of the magnets inside the domain $\mathcal{D}$) will only result in stable configurations for relatively weak forcing amplitudes, whereas in the periodic forcing case the pattern remains stable for much stronger forcing amplitudes.

The observed time-averaged stabilisation as a consequence of periodic forcing appears similar to results in the field of vibrational control. This field is based on the observation that unstable nonlinear equilibria can, under certain conditions, be approximately stabilised (time-averaged) by using a high-frequency oscillatory forcing, with a small amplitude. A well-known example is the inverted pendulum, which can be stabilised in upwards position by vertically exciting the bearing of the pendulum at a high frequency [22]. Vibrational control can also stabilise flows, *e.g.* Rayleigh-Taylor and Bénard instabilities, see [23] and references therein. However, in our experiments stabilisation occurred for a certain moderate frequency range of the forcing and it is unlikely to work for high frequencies with small amplitudes. Therefore, it is not clear yet whether the observed stabilisation is caused by the same mechanism seen in vibrational control.

In the last set of experiments, a chirp forcing was applied. Figure 4 shows that this results temporally in a flow with the same length scale as in the stationary forced experiment. There is, however, an important difference: the counterclockwise rotating vortices are larger and stronger than the clockwise rotating ones. An explanation for this phenomenon is not available yet, but this experiment shows that time-varying forcing can cause particular self-organisation in shallow-water-layer flows. In fig. 5 we have plotted the temporal evolution of the enstrophy and energy for the (inverse) chirp experiment. As time progresses we observe that these two quantities evolve along a straight line. The slope of this line is 0.85, which is close

to the slope of the line corresponding to the Taylor-Green vortex pattern $\omega_{3,4}$.

Conclusions and recommendations. – Forced Q2D free-surface flows in a shallow fluid layer have been studied experimentally for three different forcing protocols. These forcing protocols are all spatially periodic but each of them has a different time dependence. The temporal evolution of the energy and enstrophy of the free-surface flows has been evaluated in order to compare the resulting flow topology with the so-called Taylor-Green vortex patterns, which constitute a family of unstable exact solutions of the 2D Navier-Stokes equation.

For stationary forcing we observe a regular and stationary vortex pattern that is very similar to a 2D Taylor-Green vortex pattern. Time-periodic forcing results in stable but oscillating vortex patterns with vortices having a smaller size than the length scale of the forcing. Averaged in time, these patterns are also similar to a Taylor-Green vortex, yet different from the one observed for stationary forcing. This vortex pattern is remarkably stable, even for relatively strong forcing amplitudes, suggesting that this intrinsically unstable vortex pattern is stabilised when using time-periodic forcing. Finally, forcing the flow in an aperiodic way (chirp forcing) also shows the emergence of regular vortex patterns with length scales comparable to the ones observed for stationary forcing. However, contrary to the time-periodically forced case, this pattern appeared to be quasi-stationary instead of periodic. Moreover, as the symmetry of this pattern is different from the other patterns and different from the forcing, the chirp forcing appears to induce temporary self-organisation of the vortices. All experimentally observed flow patterns were analysed in the enstrophy-energy parameter space. It was found that the framework of Taylor-Green vortices is very well suited for analysing these forced vortex patterns at relatively low Reynolds numbers.

Forcing of Q2D flows with spatially periodic but time-dependent body forces seems not to have been studied before, neither analytically nor experimentally. The observations presented here show for the first time that time-varying (spatially periodic) forcing can produce approximately stable (time-averaged) vortex patterns that are intrinsically unstable when unforced, analogously to vibrational control [22].

It should be noted that the experiments reported are exploratory and suggest further studies. Although the stabilisation of otherwise unstable vortex patters by time-dependent forcing and their relation to Taylor-Green vortices has been demonstrated in principle, the mechanisms at work here are far from being understood. As a first step towards understanding, their relation to Taylor-Green vortices has been shown here. Any future work, therefore, needs to address in more detail the relationship between the stability of such vortex patterns and their energy and enstrophy evolution to the time-varying forcing. An up-to-date framework for studying this relationship is currently missing.

* * *

The authors thank Juan Pérez Munoz and Hans Zwart for help and discussions. This work, supported by NWO, and the European Communities under the contract of the Association EURATOM/FOM, was carried out within the framework of the European Fusion Programme. The views and opinions expressed herein do not necessarily reflect those of the European Commission.

REFERENCES

[1] McWilliams J. C., *J. Fluid Mech.*, **146** (1984) 21.
[2] Clercx H. J. H. and van Heijst G. J. F., *Appl. Mech. Rev.*, **62** (2009) 1.
[3] Tabeling P., *Phys. Rep.*, **362** (2002) 1.
[4] Boffetta G. and Ecke R. E., *Annu. Rev. Fluid Mech.*, **44** (2011) 427.
[5] Sommeria J., *J. Fluid Mech.*, **170** (1986) 139.
[6] Cardoso O., Marteau D. and Tabeling P., *Phys. Rev. E*, **49** (1994) 454.
[7] Marteau D., Cardoso O. and Tabeling P., *Phys. Rev. E*, **51** (1995) 5124.
[8] Cieślik A. R., Kamp L. P. J., Clercx H. J. H. and van Heijst G. J. F., *EPL*, **85** (2009) 54001.
[9] Chen Z.-M. and Price W. G., *Commun. Math. Phys.*, **179** (1996) 577.
[10] Taylor G. I., *Philos. Mag.*, **46** (1923) 671.
[11] Gotoh K. and Yamada M., *J. Phys. Soc. Jpn.*, **53** (1984) 3395.
[12] Lin S. P. and Tobak M., *Phys. Fluids*, **30** (1987) 605.
[13] Thess A., *Phys. Fluids A*, **4** (1992) 1396.
[14] Murakami Y., Fukuta H. and Gotoh K., in *Nonlinear Instability of Nonparallel Flows*, edited by Lin S. P., Phillips W. R. C. and Valentine D. T. (Springer, Berlin) 1994, pp. 320–329.
[15] van Groesen E., *Physica A*, **148** (1988) 312.
[16] van Groesen E., in *Structure, Coherence and Chaos in Dynamical Systems*, edited by Parmentier R. D. and Christiansen P. L. (Manchester University Press, Manchester) 1989, pp. 481–484.
[17] Raffel M., Willert C. E., Wereley S. T. and Kompenhans J., *Particle Image Velocimetry: A Practical Guide* (Springer, Berlin) 2007.
[18] Duran-Matute M., Trieling R. R. and van Heijst G. J. F., *Phys. Rev. E*, **83** (2011) 016306.
[19] Akkermans R. A. D., Kamp L. P. J., Clercx H. J. H. and van Heijst G. J. F., *EPL*, **83** (2008) 1.
[20] Valentine D. T., *Int. J. Numer. Methods Fluids*, **21** (1995) 155.
[21] Sommeria J. and Verron J., *Phys. Fluids*, **27** (1984) 1918.
[22] Meerkov S. M., *IEEE Trans. Autom. Control*, **25** (1980) 755.
[23] Meerkov S. M., *J. Math. Anal. Appl.*, **98** (1984) 408.